Cross fields on arbitrary surfaces :
A PDE approach based on Ginzburg-Landau theory

Pierre-Alexandre Beaufort[a,b,*], Christos Georgiadis[a], Jonathan Lambrechts[a], François Henrotte[a,b],
Christophe Geuzaine[b], Jean-François Remacle[a]

[a]*Université catholique de Louvain, iMMC, Avenue Georges Lemaitre 4, 1348 Louvain-la-Neuve, Belgium*
[b]*Université de Liège, Montefiore Institute, Allée de la Découverte 10, B-4000 Liège, Belgium*

Abstract

This paper proposes a method to compute cross fields based on the Ginzburg-Landau theory in Magnetism. According to this theory, the magnetic moment distribution in a ferromagnetic material can be regarded as a vector field with fixed norm, i.e., a directional field. The energy is the integral over the sample of the squared norm of the distribution gradient, and the sought distribution is a minimizer of this energy under the fixed norm constraint. The Ginzburg-Landau functional, which describes mathematically this situation, has two terms: the Dirichlet energy of the distribution and a term penalizing the mismatch between the fixed and actual norm of the distribution. Directional fields on surfaces are known to have a number of critical points, which are properly identified with the Ginzburg-Landau approach: the asymptotic behavior of Ginzburg-Landau problem provides well-distributed critical points over the 2-manifold, which indices are as low as possible. The central idea in this paper is to exploit this theoretical background for cross field computation on arbitrary surfaces. Such cross fields are instrumental in the generation of meshes with quadrangular elements. The relation between the topological properties of quadrangular meshes and cross fields are hence first recalled. It is then shown that a cross field on a surface can be represented by a complex function of unit norm with a number of critical points, i.e., a nearly everywhere smooth function taking its values in the unit circle of the complex plane. As maximal smoothness of the cross field is equivalent with minimal energy, the cross field problem is equivalent to an optimization problem based on Ginzburg-Landau functional. A discretization scheme with Crouzeix-Raviart elements is applied and the correctness of the resulting finite element formulation is validated on the unit disk by comparison with an analytical solution. The method is also applied to the 2-sphere where, surprisingly but rightly, the computed critical points are not located at the vertices of a cube, but at those of an anticube.

Keywords: Ginzburg-Landau theory, Cross Fields, Poincaré-Hopf, critical points (singularities), Crouzeix-Raviart, Asterisk Fields

The Finite element method (FEM) provides a powerful and versatile framework for numerical simulation, which however heavily relies on *mesh generation*, the decomposition of a geometrical region into simple shaped finite elements. In two-dimensional geometries, two kinds of elements exist: triangles and *quadrangles*. Quadrangular meshes are deemed better than triangular ones because (*i*) there are half as many quadrangles than triangles for the same number of vertices; (*ii*) it is possible to define tensorial operations on quadrangles; and (*iii*) quadrangular meshes ease the tracking of preferred directions in mesh refinement.

However, the generation of quadrangular meshes remains a challenging task, for which many strategies have been explored. Some of them, based on surface parameterization, are suitable for the generation of structured quadrangular meshes, close to regular (square) grids. A cross field may be used to determine the appropriate parameterization, either on a patch [3] or globally [4]. A cross field can also be used for partitioning the surface into a set of curvilinear quadrangular regions (a polyquad), then trivially quadrangulable [5]. The parameterization can also be deduced from a singularity graph [9]. In this paper, the primary concern is however to use cross fields as part of another meshing

---

strategy: a frontal approach firstly proposed by [1] that consists in recombining triangles into quadrangles. This can be done efficiently [2] but the quality of the quadrangles strongly depends on the node location. A heuristic to obtain well distributed nodes is to spawn them following consistent directions, such as those suggested by a smooth cross field. Such a frontal approach allows building unstructured quadrangular meshes with varying element size. Other advantages of quadrilateral meshes exist for specific finite element models: for examples, triangular plate bending elements are stiffer than quadrilateral ones with the same number of vertices

Although there exist various ways to represent discrete cross fields [10, §5], their computation generally relies on some smoothing process, possibly under constraints. For an angle-based representation, a cross field is pictured as four orthogonal or opposite vectors. From this representation, it is possible to formulate the quadrangulation as a mixed-integer problem [3]. More advanced mathematical notions such as holonomy [6] may be used as well to design cross fields. This approach requires to build a metric on the 2-manifold.

In this paper, the so-called Cartesian (complex) representation [7] is adopted. This representation naturally takes the symmetries of the cross into account, and the cross field is identified with a complex-valued function. Complex analysis gives then a large and useful background, especially about the theoretical analysis of critical points. The second term of the Ginzburg-Landau functional is controlled by a parameter depending on the local mesh size. When this parameter is small enough, the minimization of the functional results in a smooth cross field whose critical points are optimally located and whose critical points have indices with minimal absolute values, according to the theory. The previous approach closest to ours is that in [5]. It has only the energy term, but the vector field is constrained to have a norm close to the unity. Critical points are identified in this approach by computing an argument (angle) from the vector field, whereas we only need to compute the vector field norm, critical points being in our approach points where the cross field norm locally vanishes.

Our main contribution is to express the cross field problem with Ginzburg-Landau equations. Those equations rely on an interesting mathematical and physical backgrounds. In order to grasp the great understanding that Ginzburg-Landau functional provides to the cross field problem, we first recall the topological constraints of full quadrangular (and triangular) mesh in section 1 and the link with cross (and asterisk, respectively) field in section 2. In section 3, we develop the intuition of using the Ginzburg-Landau functional for the cross field problem and we give the related Ginzburg-Landau theory. We derive in section 4 a simple FEM scheme from the Ginzburg-Landau equations. Our numerical scheme is validated on the unit disk in regards with Ginzburg-Landau theory, section 5. On the 2-sphere section 6 we get a surprising but correct result. In section 7, the Ginzburg-Landau equations are modified to get better results on NACA profiles. Finally, we apply our simple finite scheme on the torus in section 8.

1. Topology of triangular and quadrilateral meshes

Assume an orientable surface $\mathcal{S}$ embedded in $\mathbb{R}^3$. Let g be the number of handles of the surface. The topological characteristic g, which is also called the genus of the surface, is the maximum number of cuttings along non-intersecting closed curves that won't make the surface disconnected. Let also b be the number of connected components of the boundary $\partial \mathcal{S}$ of the surface. The Euler characteristic of $\mathcal{S}$ is then the integer

$$\chi = 2 - 2g - b.$$

One has $\chi = 2$ for a sphere, whereas $\chi = 1$ for a disk ($b = 1$), and $\chi = 0$ for a torus ($g = 1$) or a cylinder ($b = 2$).

Consider now a mesh on $\mathcal{S}$ with n nodes (also called vertices), n_e edges and n_f facets. The Euler formula

$$\chi = n - n_e + n_f \tag{1}$$

provides a general relationship between the numbers of nodes, edges and facets in the mesh [11]. If n_b nodes (and hence n_b edges) are on the boundary $\partial \mathcal{S}$, and if the number of edges (or nodes) per facet is noted n_{evf} ($n_{evf} = 3$ for triangulations and $n_{evf} = 4$ for quadrangulations, meshes mixing triangles with quadrangles being excluded), the following identity holds : all facets have n_{evf} edges, $n_e - n_b$ edges have two adjacent facets and n_b edges have one adjacent facet. Hence the relationship

$$n_{evf} n_f = 2(n_e - n_b) + n_b. \tag{2}$$

Elimination of n_e between (2) and (1) yields

$$2n - n_b + (2 - n_{evf})n_f = 2\chi, \tag{3}$$

which is true for any triangulation or quadrangulation.

A regular mesh has only regular vertices. An internal vertex is regular if it has exactly 6 adjacent triangles or 4 adjacent quadrangles, whereas a boundary vertex is regular if it has exactly 3 adjacent triangles or 2 adjacent quadrangles. One has then

$$6(n - n_b) + 3n_b = 3n_f \quad \Rightarrow \quad n_f = 2n - n_b \tag{4}$$

and

$$4(n - n_b) + 2n_b = 4n_f \quad \Rightarrow \quad n_f = n - \frac{n_b}{2} \tag{5}$$

respectively for a regular triangulation and a regular quadrangulation. Substitution of (4) and (5) into (3) shows that only surfaces with a zero Euler characteristic can be paved with a regular mesh. If $\chi \neq 0$, irregular vertices will necessarily be present in the mesh.

The number and the index of the irregular vertices is tightly linked to the Euler characteristic χ, which is a topological invariant of the surface. We call valence of a vertex the number of facets adjacent to the vertex in the mesh. In a regular mesh, all vertices have the same valence v_{reg}. In a non regular mesh, on the other hand, a number of irregular vertices have a valence $v \neq v_{reg}$, and one notes the integer $k = v_{reg} - v$ the valence mismatch of a vertex.

Assume a quadrangulation with n_k irregular internal vertices of valence $v = 4 - k$, and n_{bk} irregular boundary vertices of valence $2 - k$, k given. All other vertices are regular. There are then $n - n_b - n_k$ regular internal vertices of valence 4, and $n_b - n_{bk}$ regular boundary vertices of valence 2, so that one can write

$$4n_f = 4(n - n_b - n_k) + 2(n_b - n_{bk}) + (4 - k)n_k + (2 - k)n_{bk}, \tag{6}$$

and the substraction of (3) with $n_{evf} = 4$ yields

$$\chi = \frac{k}{4}(n_k + n_{bk}),$$

showing that, in a quadrangulation, each irregular vertex counts for index($\mathbf{x}_i$) = $k/4$ in the Euler characteristic, a quantity called the indice of the irregular vertex $\mathbf{x}_i$.

Summing up now on different possible values for k, one can establish that a quadrangulation of a surface with Euler characteristic χ verifies

$$\chi = \sum_k \frac{k}{4}(n_k + n_{bk}) = \sum_{i=1}^{N} \text{index}(\mathbf{x}_i). \tag{7}$$

Consider, for instance, the quadrangulation of a disk, which is a surface with $\chi = 1$. A minimum of $n_1 = 4$ irregular vertices of index $1/4$ must be present. They can be located either on the boundary (vertices of valence 1) or inside the disk (vertices of valence 3), Fig. 1.

Fig. 2 shows three different quadangulations of a L-shaped domain ($\chi = 1$). Regular boundary nodes should all have a valence of 2. The mesh on the left has 6 irregular vertices located at the corners of the domain : five with index $1/4$, and one with index $-1/4$. The central mesh, on the other hand, has the minimum amount of irregular vertices, i.e. four ones of index $1/4$. The right mesh generated by recombination of a standard Delaunay triangular mesh [2] has twelve vertices of index $1/4$, and eight vertices of index $-1/4$, both on the boundary and inside the domain. Quality meshes should have as few irregular vertices as possible. In what follows, a general approach allowing to compute the position of such irregular vertices before meshing the surface is presented.

2. Why cross fields?

Cross fields are auxiliary in the generation of quadrangular meshes. We shall show that nonregular vertices defined in the previous section are precisely the critical points of a cross field, and that these critical points of the cross field can also be related to the Euler characteristic of the meshed surface. This result represents an important theoretical limit on the regularity of quadrangular meshes.
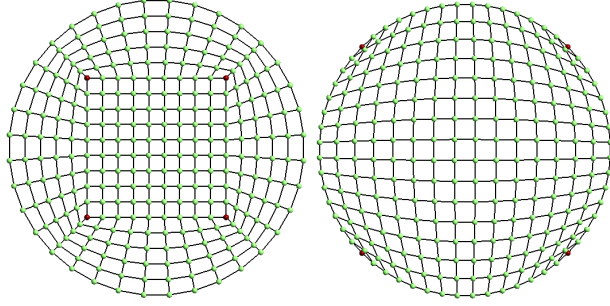
Figure 1: A quadrilateral mesh of a circle. Four irregular vertices of index 1/4 (in red) are required to obtain such a mesh. The irregular vertices may be inside the disk (left) or on its boundary (right)
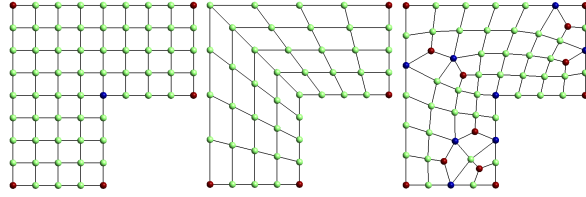

Figure 2: Different quadrangulations of a L-shaped domain. Irregular vertices of index 1/4 are displayed in red, whereas ones of index $-1/4$ are displayed in blue. The sum of the indices of the irregular vertices is equal to $\chi = 1$ in all cases.

2.1. Continuity

A cross field f is a field defined on a surface $\mathcal{S}$ with values in the quotient space S^1/Q, where S^1 is the circle group and Q is the group of quadrilateral symmetry. Pictorially, it associates to each point of the surface $\mathcal{S}$, which has to be meshed, a cross made of four unit vectors that are orthogonal with each others in the tangent plane $T\mathcal{S}$ of the surface.

A surface $\mathcal{S}$ can be identified with its tangent space in any neighborhood $\sigma \subset \mathcal{S}$ that is sufficiently small to have curvature effects negligible. This local identification of the surface with a vector space endows it with a natural parallel transport rule, so that the angular differential $\mathrm{d}\theta_f(\mathbf{x}_a, \mathbf{x}_b)$ can be defined as the minimal angle, with its sign, between the branches of $f(\mathbf{x}_a)$ and any of the branches of $f(\mathbf{x}_b)$ for any pair of points $\mathbf{x}_a, \mathbf{x}_b \in \sigma$ where f is defined, Fig. 3. Taking now as reference the cross $f(\mathbf{x}_a)$, an angular coordinate

$$\theta_f(\mathbf{x}) = \mathrm{d}\theta_f(\mathbf{x}_a, \mathbf{x}) \tag{8}$$

can be defined for crosses in σ. The cross field f is deemed continuous (regular) at $\mathbf{x}_b$ if the limit

$$\lim_{\mathbf{x} \to \mathbf{x}_b} \theta_f(\mathbf{x}) = \theta_f(\mathbf{x}_b) \tag{9}$$

exists (i.e. is unique). It is then equal to $\theta_f(\mathbf{x}_b)$. Isolated points $\mathbf{x}_i$, $i = 1 \ldots N$, of $\mathcal{S}$ where the limit (9) does not exist are called critical points or zeros of the cross field.
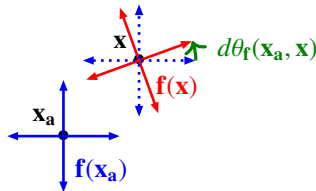

Figure 3: Diffential function $\mathrm{d}\theta_f$.

4

2.2. Index and degree

Although defined locally, the notion of continuity gives unexpectedly valuable information about the topology of $\mathcal{S}$, which is a nonlocal concept. To see this, consider a cross field f defined on a quadrangular element delimited by four (possibly curvilinear) edges. Assume the cross field is parallel to the four edges (i.e. one of the four branches of the cross is parallel to the tangent vector of the edge at each point of the edge, except the extremities) and prolongates smoothly inside the quadrangle. This field is discontinuous at corners where edges do not meet at right angle, but it is continuous everywhere else. Making the same construction for all elements of a quadrangular mesh, one obtains a cross field f topologically identified with the quadrangular mesh, and that is continuous everywhere except at the vertices of the mesh. This field has thus got isolated critical points at mesh vertices, but not all critical points have the same significance. Some critical points have a specific topological value, associated with the notion of index.

To introduce the notion of index, an angular coordinate needs to be defined for points in a neighborhood σ_i of a critical point $\mathbf{x}_i$. Picking up an arbitrary regular point $\mathbf{x}_a \in \sigma_i$, $\mathbf{x}_a \neq \mathbf{x}_i$, the local unit vector basis

$$\mathbf{e}_1 = \frac{\mathbf{x}_a - \mathbf{x}_i}{|\mathbf{x}_a - \mathbf{x}_i|} \quad , \quad \mathbf{e}_2 = \mathbf{n} \times \mathbf{e}_1,$$

with $\mathbf{n}$ the normal to $\mathcal{S}$, is constructed, and hence a local polar coordinate system

$$r(\mathbf{x}) = |\mathbf{x} - \mathbf{x}_i| \quad , \quad \theta(\mathbf{x}) = \mathrm{atan2}\big((\mathbf{x} - \mathbf{x}_i) \cdot \mathbf{e}_2, (\mathbf{x} - \mathbf{x}_i) \cdot \mathbf{e}_1\big) \tag{10}$$

can be defined for points in σ_i.

A circular curve C_i of infinitesimal radius centered around the vertex $\mathbf{x}_i$ is now considered. As the angles $\theta(\mathbf{x})$ (10) and $\theta_f(\mathbf{x})$ (8) are precisely the elements of the groups S^1 and S^1/Q, respectively, the cross field on C_i can be regarded as a mapping

$$f : S^1 \mapsto S^1/Q. \tag{11}$$

The mapping is continuous, since C_i circles around the critical point $\mathbf{x}_i$, but it does not cross it. The index of f at $\mathbf{x}_i$ is the degree of the mapping (11), i.e. the number of times the codomain wraps around the domain under the mapping. Its algebraic expression is easily expressed in terms of the angles θ and θ_f as

$$\mathrm{index}(\mathbf{x}_i) = \frac{1}{2\pi} \oint_{C_i} \mathrm{d}\theta_f$$

where 2π is $\oint_{C_i} \mathrm{d}\theta$. In case of a vertex $\mathbf{x}_i$ of valence v_i, i.e. a vertex adjacent to v_i quadrangular elements, the integral evaluates as

$$\mathrm{index}(\mathbf{x}_i) = \frac{1}{2\pi} \sum_{p=1}^{v_i} \left(\alpha_p - \frac{\pi}{2} \right) = \frac{1}{2\pi} (2\pi - v_i \frac{\pi}{2}) = \frac{4 - v_i}{4}, \tag{12}$$

where the α_p's are the angles of the v_i quadrangular elements adjacent to the considered vertex $\mathbf{x}_i$, and where the obvious relationship $\sum_{p=1}^{v_i} \alpha_p = 2\pi$ has been used. The cross field f has index 0 at vertices adjacent to four quadrangular elements, whereas it has index $1/4$ $(-1/4)$ at vertices adjacent to 3 (5, respectively) quadrangular elements meet, Fig. 4. As one sees, the index is a topological characteristic of the cross field f at the critical point $\mathbf{x}_i$. It does not depend on the choice of the curve C_i, nor on the choice of an angular reference for the angles $\theta(\mathbf{x})$ and $\theta_f(\mathbf{x})$.

2.3. Poincaré-Hopf theorem

Equation (12) relates the index of the cross field at a critical point $\mathbf{x}_i$ with one fourth of valence $k_i = 4 - v_i$ of the corresponding mesh vertex. This result can be combined with the algebraic topology result of previous section (7) that each internal irregular vertex of valence k_i counts for $k_i/4$ in the Euler characteristic of the underlying surface. This yields the relationship

$$\sum_{i=1}^{N} \mathrm{index}(\mathbf{x}_i) = \chi \tag{13}$$

for the critical points of a cross field f defined on a surface $\mathcal{S}$.
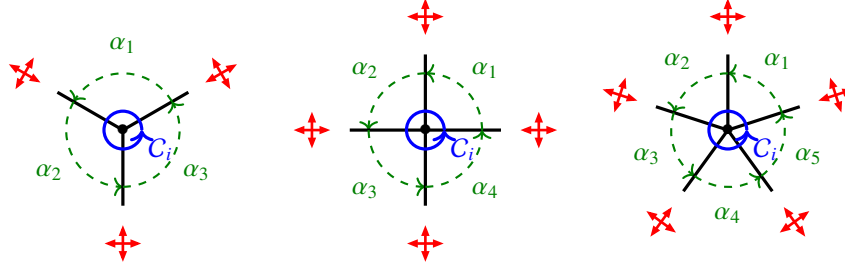
Figure 4: Illustration of vertices where the indices of the cross field (in red) are respectively $1/4, 0$ and $-1/4$, from left to right. The index only depends on the number of quadrangles that are adjacent to the vertex, independently of the values of the angles α_p, which don't need to be identical as they are in the figure.

This is a generalization Poincaré-Hopf theorem, which states that the sum of the indices of the critical points of a *vector* field $\mathbf{v}$ defined on a surface $\mathcal{S}$ without boundary is equal to the Euler characteristic of the surface. This famous theorem draws an unexpected and profound link between two apparently distinct areas of mathematics, topology and analysis. Whereas vector fields have integer indices at critical points, cross fields have indices that are multiples of $1/4$. Still the topological relationship (13) of Poincaré-Hopf holds in both cases. Actually, our developments reach same inferences as [8].

3. Cross field computation : the planar case

We introduce the representation of a cross field by means of a vector field. From this representation, we derive the problem to solve that corresponds to minimize Ginzburg-Landau functional. Its asymptotic behavior provides suitable critical points, if any.

3.1. Vector representation of cross fields

Only scalar quantities can be compared at different points of a manifold. For the comparison or, more generally, for differential calculus with nonscalar quantities like cross fields, a parallel transport rule needs to be defined on the manifold. On a surface (two-manifold), this rule can take the form of a regular vector field which gives at each point the direction of the reference angle 0. Poincaré-Hopf theorem says that such a field does not exist in general, and in particular on manifolds whose Euler characteristic is not zero. The situation is however easier in the planar case. A global Cartesian coordinate frame can always be defined over the plane, and be used to evaluate the orientation of the cross field. We shall therefore expose the cross field computation method in the planar case, and then generalize to nonplanar surfaces, where we will have to deal with local reference frames, in a subsequent section.

A cross $f(\mathbf{x})$ is an element of the group S^1/Q, which can be represented by the angle $\theta_f(\mathbf{x})$ it forms with the local reference frame. Yet, due to the quadrilateral symmetry, four different angles in $[0, 2\pi[$ represent the same cross field $f(\mathbf{x})$. Let for instance the angles $\theta_1 = 0$ and $\theta_2 = \pi/2$ represent the same cross. The average $(\theta_1 + \theta_2)/2 = \pi/4$ represents another cross, whereas the difference $\theta_2 - \theta_1 = \pi/2$ is not zero. So, we have $\frac{1}{2}(x+x) \neq x$ and $x-x \neq 0$, which clearly indicates that the values of the cross field f do not live in a linear (affine) space. This makes the representation by θ_f improper for finite element interpolation. The solution is two-fold. First, the angle θ_f is multiplied by four, so that the group S^1/Q is mapped on the unit circle S^1, and the cross f is therefore represented by a unit norm vector $\mathbf{f}$. Then, the vector is represented in components in the reference frame as

$$\mathbf{f} = (\cos 4\theta_f, \sin 4\theta_f) \equiv (f_1, f_2).$$

This vector may be represented by a complex-valued function

$$f = f_1 + i\, f_2$$

This representation corresponds to a vector field that is described by a complex exponential which argument is $4\,\theta$. A cross field is thus depicted by the fourth roots of a (unit) complex number. This observation may be generalized for directional fields with n symmetries [10, §5.2].

6

3.2. Laplacian smoothing

Computing the cross field f consists thus now of computing the vector field representation $\mathbf{f}$, which obviously lives in a linear space (a 2D plane). The components of $\mathbf{f}$ are fixed on the boundaries of $\Gamma = \partial S$ so that the crosses are parallel with the exterior normal vector $\mathbf{n} = (\cos \theta_n, \sin \theta_n)$ i.e.

$$\mathbf{f} = (\cos 4\theta_n, \sin 4\theta_n) \quad \text{on } \Gamma.$$

Propagating $\mathbf{f}$ inside S is here done by solving a Laplacian problem. Even though the vector representation $\mathbf{f}$ is unitary on Γ, it tends to drift away from S^1 inside the domain. The computed finite element solution $\mathbf{f}$ lies therefore outside the unit circle and must be projected back on S^1 to recover the angle

$$\theta_f = \frac{\text{atan2}(f_2, f_1)}{4}.$$

Due to the multiplication by 4, the indices of the critical points of the vector field $\mathbf{f}$ verify

$$\sum_{i=1}^{N} \text{index}(\mathbf{x}_i) = 4\chi. \tag{14}$$

3.3. The Ginzburg-Landau model

Numerical experiments show that the norm of the vector field $\mathbf{f}$ computed by Laplacian smoothing (see previous section) decreases quite rapidly as one moves away from the boundary ∂S, leaving in practice large zones in the bulk of the computational domain where the solution is small, and the computed cross field inaccurate, Fig. 5a. A more satisfactory formulation consists of ensuring that the norm of $\mathbf{f}$ remains unitary over the whole computational domain, Fig. 5b. This problem can be formulated in variational form in terms of the Ginzburg-Landau functional

$$E(f_1, f_2) = \underbrace{\frac{1}{2} \int_S \left(|\nabla f_1|^2 + |\nabla f_2|^2 \right) dS}_{\text{smoothing}} + \underbrace{\frac{1}{4\epsilon^2} \int_S \left(f_1^2 + f_2^2 - 1 \right)^2 dS}_{\text{penality}}. \tag{15}$$

The first term minimizes the gradient of the cross field and is therefore responsible for the laplacian smoothing introduced in the previous section. The second term is a penalty term that vanishes when $\mathbf{f} \in S^1$. The penalty parameter ϵ, called *coherence length*, has the dimension of a length. The Euler-Lagrange equations of the functional (15) are the quasi-linear PDE's

$$\nabla^2 f_i - \frac{1}{\epsilon^2} \left(f_1^2 + f_2^2 - 1 \right) f_i = 0 \quad i = 1, 2. \tag{16}$$

called Ginzburg-Landau equations. If ϵ is small (enough) with respect to the dimension of S, then $\mathbf{f}$ is of norm 1 everywhere but in the vicinity of the isolated critical points $\mathbf{x}_i^c$.

The asymptotic behavior of Ginzburg-Landau energy can be written as

$$E = \pi \left(\sum_{i=1}^{N} \text{index}(\mathbf{x}_i^c)^2 \right) \log(1/\epsilon) + W + O(1/|\log \epsilon|). \tag{17}$$

with

$$W = -\pi \sum_{i=1}^{N} \sum_{\substack{j=1 \\ j \neq i}}^{N} \text{index}(\mathbf{x}_i^c) \, \text{index}(\mathbf{x}_j^c) \log |\mathbf{x}_i^c - \mathbf{x}_j| + \mathcal{R} \tag{18}$$

as $\epsilon \to 0$ (see [12], Introduction, Formulae 11 and 12).

In asymptotic regime, the energy is thus composed of three terms. The first term of (17) blows up as $\epsilon \to 0$, i.e. energy becomes unbounded if critical points are present. When ϵ is small, this first term dominates, and one is essentially minimizing $\sum_{i=1}^{N} \text{index}(\mathbf{x}_i^c)^2$ with the constraint (14). This indicates that a critical point of index 2 has a cost of 4 in terms of energy, whereas 2 critical points of index 1 have a cost of 2. All critical points should therefore

7

be of index ± 1, and their number should be $N = 4\,|\chi|$. This is indeed good news for our purpose : good cross fields should have few critical points of lower indices.

The second term of (17) is the *renormalized energy W* (18). It remains bounded when ϵ tends to 0. The double sum in W reveals the existence of a logarithmic force between critical points. The force is attractive between critical points with indices of opposite signs, and repulsive between critical points with indices of the same signs. The second term in (18) is more complicated and is detailed in [12]. Basically, $\mathcal{R}$ represents a repulsing force that forbids critical points to approach the boundaries.

Finally, the third term in (17) vanishes as $\epsilon \to 0$. At the limit, all energy is thus carried by the critical points of the field. All this together allows to believe that Ginzburg-Landau model is a good choice for computing cross fields. It produces few critical points, which are moreover well-distributed over the domain.

a. Minimizing Dirichlet energy.   b. Minimizing Ginzburg-Landau energy.
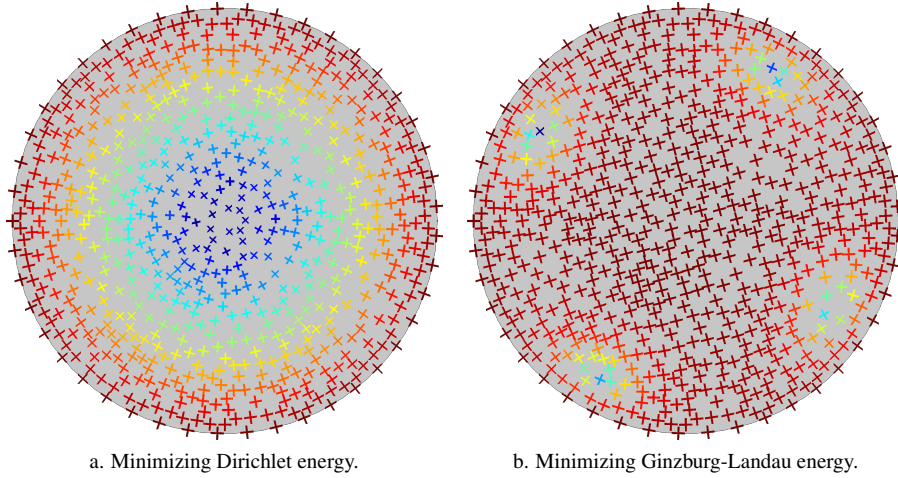
Figure 5: Cross field over a disk. The color describes the field norm: blue is close to zero, red close to unity.

4. Computation of cross fields: nonplanar generalization

The finite element computation method for cross fields is now generalized to the case of nonplanar surfaces. Consider the conformal triangulation $\mathcal{S} = \cup_{ijk}\Omega_{ijk}$ of a nonplanar surface manifold $\mathcal{S}$, each triangle Ω_{ijk} being defined by the vertices $\mathbf{p}_i$, $\mathbf{p}_j$ and $\mathbf{p}_k$. Since no global reference frame exists on a nonplanar surface, a local reference frame is associated to each edge of the triangulation. Let e^p be the pth edge of the mesh, joining nodes $\mathbf{p}_i$ and $\mathbf{p}_j$, and $\mathbf{n}^p$ be the average of the normals vectors of the two triangles adjacent to e^p. The vectors

$$\left\{\mathbf{e}^p = \mathbf{p}_j - \mathbf{p}_i, \mathbf{t}^p = \mathbf{n}^p \times \mathbf{e}^p\right\}$$

form a local frame $\{\hat{e}^p, \hat{t}^p\}$ which enables the representation of the connector values of the discretized cross field $\mathbf{f}$,

$$f_1^p = \cos 4\theta_f^p \quad , \quad f_2^p = \sin 4\theta_f^p,$$

which are attached to the center of the edges of the triangulation. Actually, θ_f^p is assumed to be the same along $\boldsymbol{e}^p$ within both planes of triangles sharing e^p. This assumption eases computations and gives a planar-like representation, Fig. 6a.

As the connector values are attached to the edges of the mesh, and not to the nodes, Crouzeix-Raviart interpolation functions are used instead of conventional Lagrange shape functions [13]. The Crouzeix-Raviart shape functions ω^p equal 1 on corresponding edge e^p, and -1 on the opposite vertices (Fig. 7) in the two adjacent triangular elements. They are polynomial and their analytic expression in the reference triangle $\{\xi \in [0, 1], \ \eta \in [0, 1 - \xi]\}$ reads

$$\omega^{(1)}(\xi, \eta) = 1 - 2\eta \quad , \quad \omega^{(2)}(\xi, \eta) = 2(\xi + \eta) - 1 \quad , \quad \omega^{(3)}(\xi, \eta) = 1 - 2\xi,$$

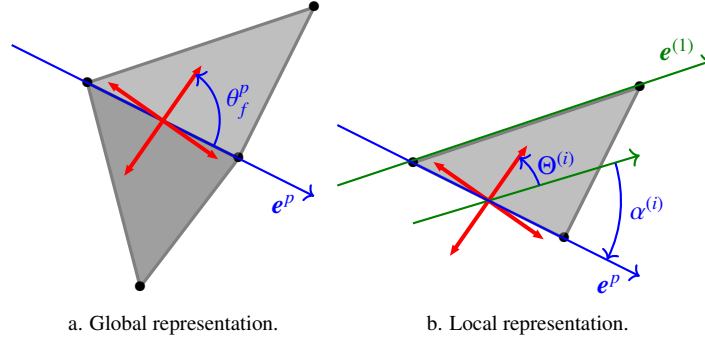8

a. Global representation. b. Local representation.

Figure 6: Cross field over the pth edge of a mesh.

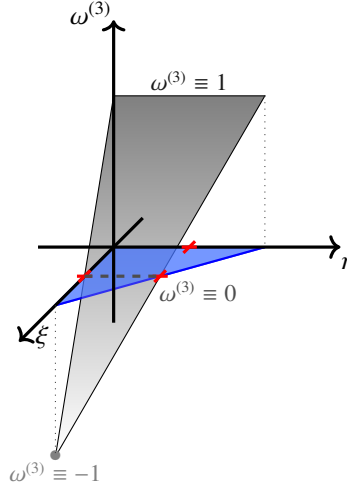where indices $(1), (2)$ and (3) enclosed in parentheses denote the local edge numbering in the considered triangular element.

Figure 7: Third Crouzeix-Raviart function shape (shaded in grey) over reference triangle (in blue).

Each of the three edges of a triangle Ω_{ijk} has its own local reference frame. If one is to interpolate expressions involving the vector field $\mathbf{f}$ over this element, the three edge-based reference frames have to be appropriately related with each other [14]. We arbitrarily take the reference frame of the first edge of the element as reference, and express the angular coordinate of the two other edges in function of this one with the relationships (Fig. 6b)

$$\Theta^{(1)} = \theta_f^{(1)} \quad , \quad \Theta^{(2)} = \theta_f^{(2)} + \alpha^{(2)} \quad , \quad \Theta^{(3)} = \theta_f^{(3)} + \alpha^{(3)}.$$

Thus, the 6 local unknowns of triangle Ω_{ijk} can be expressed as a function of the 6 edge unknowns by

$$\underbrace{\begin{pmatrix} \cos 4\Theta^{(1)} \\ \cos 4\Theta^{(2)} \\ \cos 4\Theta^{(3)} \\ \sin 4\Theta^{(1)} \\ \sin 4\Theta^{(2)} \\ \sin 4\Theta^{(3)} \end{pmatrix}}_{} \equiv \underbrace{\begin{pmatrix} F_1^{(1)} \\ F_1^{(2)} \\ F_1^{(3)} \\ F_2^{(1)} \\ F_2^{(2)} \\ F_2^{(3)} \end{pmatrix}}_{\mathbf{F}^{ijk}} = \underbrace{\begin{bmatrix} 1 & 0 & 0 & 0 & 0 & 0 \\ 0 & \cos 4\alpha^{(2)} & 0 & 0 & \sin 4\alpha^{(2)} & 0 \\ 0 & 0 & \cos 4\alpha^{(3)} & 0 & 0 & \sin 4\alpha^{(3)} \\ 0 & 0 & 0 & 1 & 0 & 0 \\ 0 & -\sin 4\alpha^{(2)} & 0 & 0 & \cos 4\alpha^{(2)} & 0 \\ 0 & 0 & -\sin 4\alpha^{(3)} & 0 & 0 & \cos 4\alpha^{(3)} \end{bmatrix}}_{\mathbf{R}^{ijk}} \underbrace{\begin{pmatrix} f_1^{(1)} \\ f_1^{(2)} \\ f_1^{(3)} \\ f_2^{(1)} \\ f_2^{(2)} \\ f_2^{(3)} \end{pmatrix}}_{\mathbf{f}^{ijk}}$$

9

and we have the interpolation

$$F_1^{ijk}(\xi, \eta) = \sum_{i=1}^{3} \omega^{(i)}(\xi, \eta) \, F_1^{(i)} \quad , \quad F_2^{ijk}(\xi, \eta) = \sum_{i=1}^{3} \omega^{(i)}(\xi, \eta) \, F_2^{(i)}$$

for the vector field $\mathbf{f}$ in the triangle Ω_{ijk}.

A Newton scheme is proposed to converge to the solution. The Newton iteration at stage n for solving (16) consists of solving:

$$\nabla^2 \begin{pmatrix} f_1 \\ f_2 \end{pmatrix}_n - \frac{1}{\epsilon^2} \begin{pmatrix} 3f_1^2 + f_2^2 - 1 & 2f_1 f_2 \\ 2f_1 f_2 & f_1^2 + 3f_2^2 - 1 \end{pmatrix}_{n-1} \begin{pmatrix} f_1 \\ f_2 \end{pmatrix}_n = -\frac{2}{\epsilon^2} \begin{pmatrix} f_1^3 + f_1 f_2^2 \\ f_1^2 f_2 + f_2^3 \end{pmatrix}_{n-1} \tag{19}$$

The 6×6 elementary matrix $\mathbf{K}^{ijk}$ and the 6×1 elementary vector $\mathbf{B}^{ijk}$ of element Ω_{ijk} are then given by

$$\mathbf{K}^{ijk} = \begin{bmatrix} \left(\int_{\Omega_{ikj}} \nabla\omega_m \cdot \nabla\omega_n + \frac{1}{\epsilon^2}(3F_1^2 + F_2^2 - 1)\omega_m\omega_n \, d\Omega \right)_{m,n=1...3} & \left(\int_{\Omega_{ijk}} \frac{2}{\epsilon^2}F_1 F_2\omega_m\omega_n \, d\Omega \right)_{m,n=1...3} \\ \left(\int_{\Omega_{ijk}} \frac{2}{\epsilon^2}F_1 F_2\omega_m\omega_n \, d\Omega \right)_{m,n=1...3} & \left(\int_{\Omega_{ikj}} \nabla\omega_m \cdot \nabla\omega_n + \frac{1}{\epsilon^2}(F_1^2 + 3F_2^2 - 1)\omega_m\omega_n \, d\Omega \right)_{m,n=1...3} \end{bmatrix} \tag{20}$$

and

$$\mathbf{B}^{ijk} = \begin{pmatrix} \left(\int_{\Omega_{ijk}} \nabla F_1 \cdot \nabla\omega_n + \frac{1}{\epsilon^2}(F_1^3 + F_2^2 - F_1)\omega_n \, d\Omega \right)_{n=1...3} \\ \left(\int_{\Omega_{ijk}} \nabla F_2 \cdot \nabla\omega_n + \frac{1}{\epsilon^2}(F_1^2 + F_2^3 - F_2)\omega_n \, d\Omega \right)_{n=1...3} \end{pmatrix}. \tag{21}$$

It is then necessary to transform those elementary matrix and vector in the reference frames of the edges as

$$\mathbf{k}^{ijk} = (\mathbf{R}^{ijk})^T \mathbf{K}^{ijk} \mathbf{R}^{ijk} \quad \text{and} \quad \mathbf{b}^{ijk} = (\mathbf{R}^{ijk})^T \mathbf{B}^{ijk}.$$

Then, standard finite element assembly can be performed. Boundary conditions are simply

$$f_1^p = 1 \quad , \quad f_2^p = 0$$

on every edge e^p of ∂S. This nice simplification is due to the fact that unknowns are defined on the reference frame of the edges.

5. Numerical validation: the unit disk

We compute the analytical location of critical points of a directional field defined on the unit disk. The calculations are based on the Ginzburg-Landau results, described in section 3.3. The numerical location obtained by our FEM is compared to the analytical one.

Let S be the open unit disk in $\mathbb{R}^2$, i.e.

$$S := \left\{ (x_1; x_2) \in \mathbb{R}^2 \mid x_1^2 + x_2^2 < 1 \right\}$$

For a star-shaped planar domain such as S with a smooth boundary ∂S of exterior normal ν and tangent τ, which vector field has d critical points of index $+1$ at $X^c = \{\mathbf{x}_1^c, ..., \mathbf{x}_d^c\} \in S$, the asymptotic energy E_ϵ (in complex form) becomes

$$E_\epsilon \underset{\epsilon \to 0}{\longrightarrow} \pi d \, |\log(\epsilon)| + W(X^c) + O(\epsilon) \tag{22}$$

where $W(X^c)$ is the renormalized energy

$$W(X^c) = -\pi \sum_{i \neq j} \log |\mathbf{x}_i^c - \mathbf{x}_j^c| + \frac{1}{2} \int_{\partial S} \Phi \, f \times \nabla f \cdot \tau \, ds - \pi \sum_i R(\mathbf{x}_i^c) \tag{23}$$

where Φ is given by the following Neumann problem

$$\left.\begin{aligned}
\nabla^2 \Phi(\mathbf{x}) &= 2\pi \sum_{i=1}^{d} \delta(\mathbf{x} - \mathbf{x}_i^c) \quad \text{in} \quad \mathcal{S} \\
\nabla\Phi \cdot \nu &= f \times \nabla f \cdot \tau \qquad \text{on} \quad \partial\mathcal{S}
\end{aligned}\right\} \tag{24}$$

and R is the regular part of Φ:

$$R(\mathbf{x}) = \Phi(\mathbf{x}) - \sum_{i=1}^{d} \log |\mathbf{x} - \mathbf{x}_i^c| \tag{25}$$

E_ϵ is minimum when the critical points are located appropriately, i.e. when (23) is minimum. The renormalized energy W corresponds to the Ginzburg-Landau energy (22) when the singular core energy $\pi d |\log(\epsilon)|$ has been removed. Since W depends only on the location of the critical points, it is possible to compute their location in the case of the unit disk, in order to get an optimal directional field.

The minimum of W is obtained by sampling points within the unit disk. It is assumed that the d critical points exhibit the d symmetries of their group (the quadrilateral group in the case $d = 4$). In other words, it means that they are at the same distance r^c from the center of the disk (i.e. the origin $(0; 0)$), and separated two-by-two with an angle of $2\pi/d$ radians.

The Neumann problem (24) is solved by decomposing $\Phi = \Phi^0 + \Phi^1$. The first term Φ^0 is the Green function of a two-dimensional Laplacian operator, while the second one Φ^1 is obtained by separation of variables (r, θ). The solution is then

$$\Phi(r, \theta) = \sum_{i=1}^{d} \left[\underbrace{\log |r \cos(\theta) - \mathbf{x}_i^c|}_{\Phi_i^0} + \underbrace{\sum_{n=1}^{\infty} A_{i,n} r^n \cos(n\theta)}_{\Phi_i^1} \right] \tag{26}$$

where $A_{i,n}$ depends on the location of the i-th critical point. It is possible to show that he second term of (23) is zero, Appendix A.2. The analytic solution of Neumann problem is derived into the Appendix A.1.

The evaluation of W consists of computing the first and last terms, by sampling the disk. The sampling is done by selecting d critical points spaced by $2\pi/d$ radians. The distance r^c is sampled between zero and one. The distance r^{c^*} which gives the lowest value of W defines the location of the critical points. A Python script performs the evaluations and returns the optimal distance r^{c^*}, Fig. 8.

The corresponding directional fields are computed, and their critical point locations are compared with circles which radii correspond to r^{c^*}, Fig. 9. The location of critical points are really close to the estimation based on the analytical solution of $W(X^c)$ in the case of the unit circle. They tend to draw the corners of the polygon of symmetry: a square in the case of the cross field, Fig. 9a and a regular hexagon for the asterisk field, Fig. 9b. The critical points are quite close to the unit circle. The more critical points, the closer to the unit circle they are. We understand that the repulsion term is stronger than the regularization term within the domain. The regularization term is only able to forbid critical points to be on the boundary, i.e. the unit circle.

6. A surprising result: the sphere

Let us compute the cross field on a unit sphere. The sphere has no boundary so we choose randomly one edge of the mesh and fix the cross field for this specific edge. The mesh of the sphere is made of 2960 triangles (see Fig. 10). A value of $\epsilon = 0.1$ was chosen for the computation. A total of 29 Newton iterations were necessary to converge, by reducing the residual norm to 10^{-12}. The location of the 8 critical points is indeed not what we expected: our initial intuition was that critical points would be located at the corners of an inscribed cube of side $1/\sqrt{3}$. In all our computations i.e. while changing the mesh and ϵ, critical points are located on two squares of side $1/\sqrt{3}$, those two squares being tilded by 45 degrees around their common axe (see Fig. 10). Equilateral triangle patterns are formed between critical points that belong to both squares. In reality, our solution is the right solution. In the asymptotic
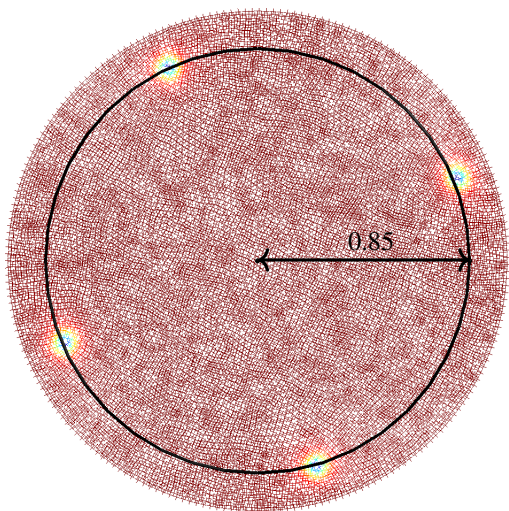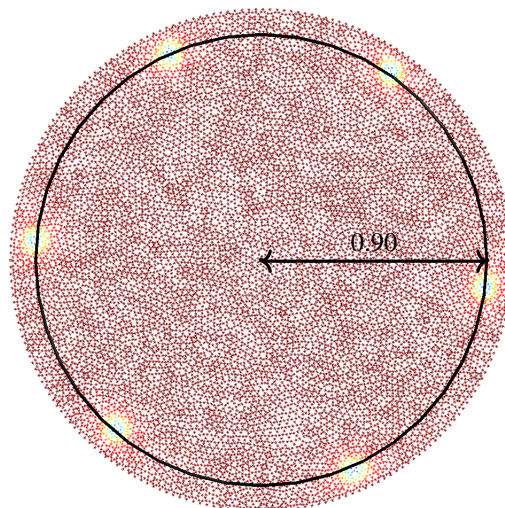
11
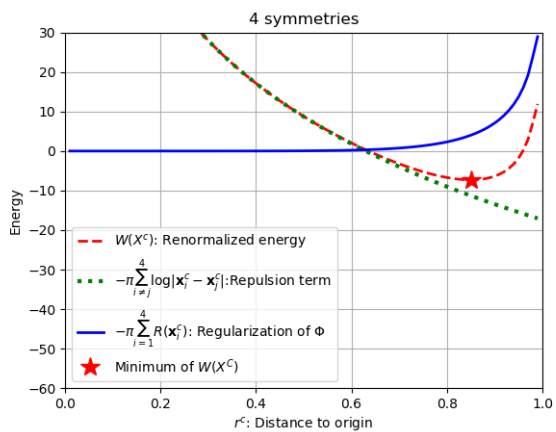
a. Four critical points: $r^{c*} = 0.85$.
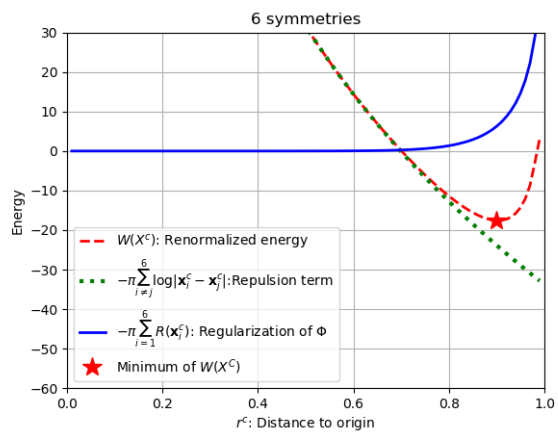
b. Six critical points: $r^{c*} = 0.90$.

Figure 8: Python evaluations of renormalized energy W for different X^c on a unit disk $\mathcal{S}$.

a. Cross field.

b. Asterisk field.

Figure 9: FEM computations of direction fields on a unit disk $\mathcal{S}$: the critical points are in blue areas.
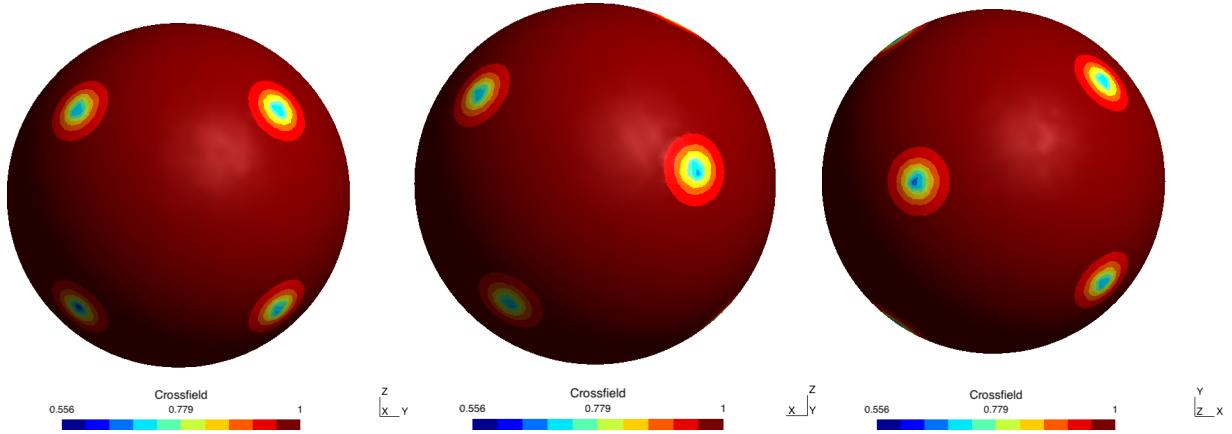
Figure 10: Mesh of the sphere. Colors correspond to the 2-norm $\|\mathbf{f}\|$ of the cross field. The 8 critical points are located on two squares of side $1/\sqrt{3}$, which corresponds to the size of the inscribed cube. The two squares are tilted by 45 degrees.

regime, the location $\mathbf{x}_i^c$ of the 8 critical points tends to minimize $-\sum_i \sum_{i \neq j} \log |\mathbf{x}_i^c - \mathbf{x}_j^c|$ (see Equations (17) and (18)). We have thus computed $-\sum_i \sum_{i \neq j} \log |\mathbf{x}_i^c - \mathbf{x}_j^c|$ for tilting angles ranging from 0 to $\pi/2$. Fig. 11 shows clearly that the minimum of the energy corresponds to an angle of $\pi/4$, which is exactly what is found by the finite element formulation. Fig. 12 shows the cross field as well as the separatrices. The separatrices were computed "by hand".
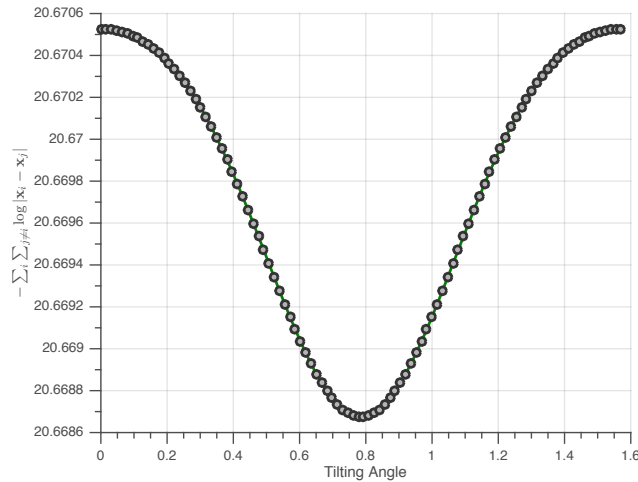
Figure 11: Energy vs. tilting angle for the sphere. The minimum corresponds to a titing angle of $\pi/4$.

The solution that has been found is related to what is called the Whyte's problem [15, 16] that consists of finding N points on the sphere which positions maximize the product of their distances. The critical points are called *logarithmic extreme points* or *elliptic Fekete points* [17].

The specific configuration that corresponds to $N = 8$ is called an anticube (or square antiprism) and is exactly the one that was found numerically.

In the case of an asterisk field, the critical points are the summits of an icosahedron, which is the solution of Whyte's problem for $N = 12$. This superb result shows that it is indeed possible to use cross fields not only for building quadrangles but also to build equilateral triangles.

Actually, it is possible to show that the critical points computed over the sphere by Ginzburg-Landau correspond to the solution of Whyte's problem for any even value of N [19].
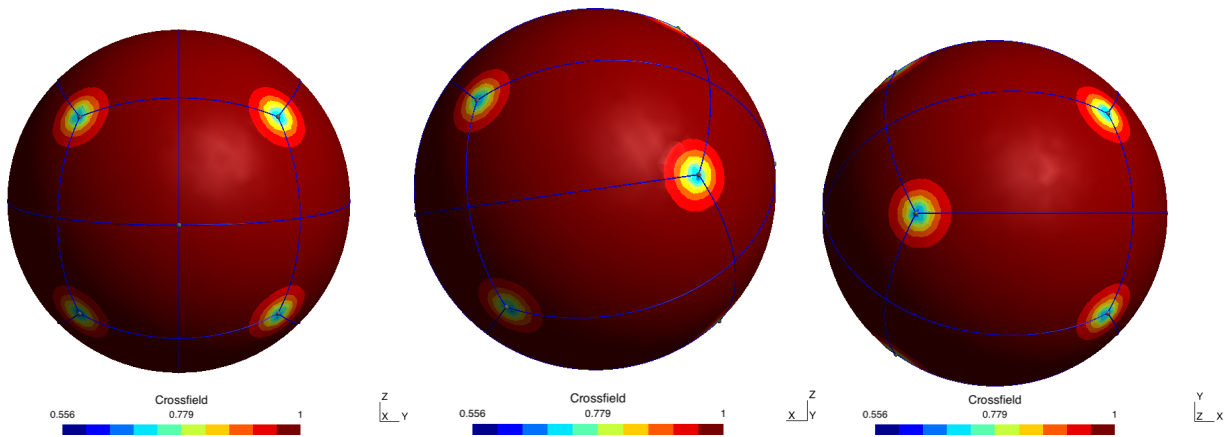
13

Figure 12: Separatrices from cross field.
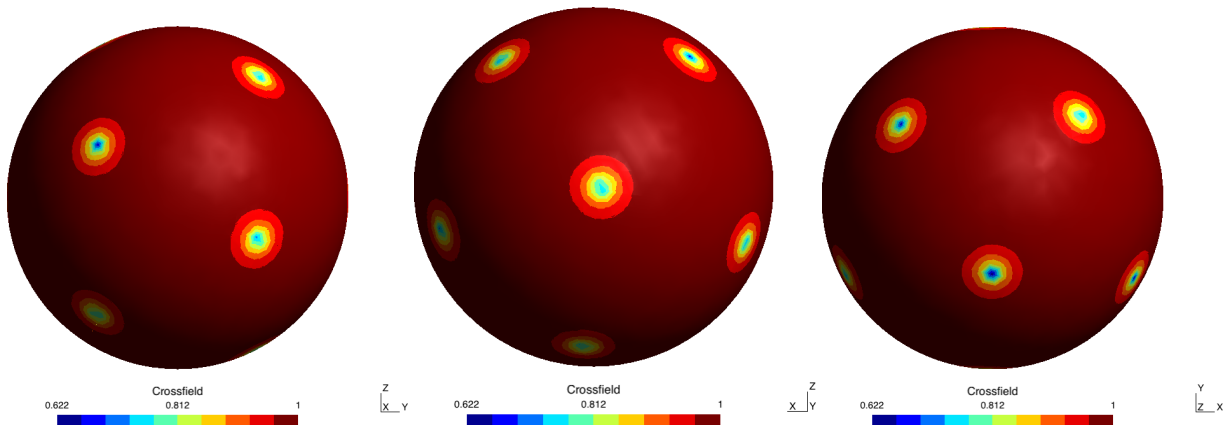

Figure 13: Asterisk field (6 symmetries) which the critical points correspond to the corners of an icosahedron.

7. Weak boundary conditions

In this section, we have computed the graph of singularities of a standard CFD test case: a three component wing domain with $\chi = -2$. This example is very similar to the one presented by Kowalski et al in [5]. The solution has been computed on a non uniform triangular mesh of about $15,000$ triangles. The graph of singularities has been depicted on Fig. 14. Weak boundary conditions have been applied to the different components of the wing where a penalization
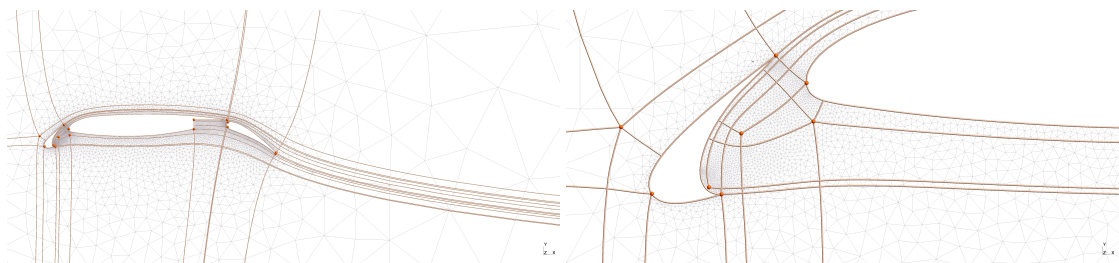
Figure 14: Graph of singularities for the three component wing. Right figure is a zoom on the leading edge slat.
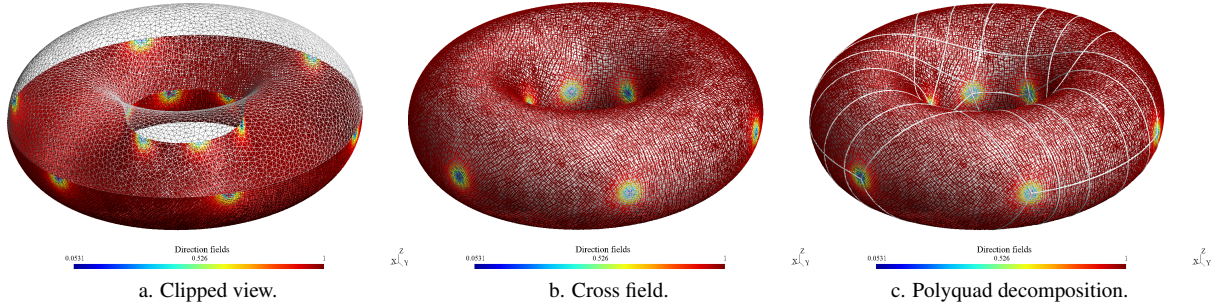
14

Figure 15: FEM ($\epsilon = 0.06$) cross field on a torus discritized by 20612 triangles. Twelve critical points of opposite indices ($\pm 1/4$).

replaces the strong imposition of f on boundaries. A new term is thus added to Energy (15) for taking into account boundary conditions:

$$E(f_1, f_2) = \frac{1}{2} \int_{\mathcal{S}} \left(|\nabla f_1|^2 + |\nabla f_2|^2 \right) d\mathcal{S} + \frac{1}{4\epsilon^2} \int_{\mathcal{S}} \left(f_1^2 + f_2^2 - 1 \right)^2 d\mathcal{S} + \frac{L}{2\epsilon^2} \int_{\partial\mathcal{S}} \left[(f_1 - \bar{f}_1)^2 + (f_2 - \bar{f}_2)^2 \right] d\partial\mathcal{S} \qquad (27)$$

where $\bar{f}_1$ and $\bar{f}_2$ are values of the crosses that are weakly imposed on the boundary and L the characteristic size of the problem. This new treatment allows singularities to migrate on the boundary, making their repulsive action finite. Figure 14 clearly shows that effect: a singularity of index 1/4 sits on the leading edge of the slat, allowing a clean decomposition of the domain. The same migration is also observed on the leading edge of the profile. A strong imposition of boundary conditions naturally leads to singularities that are very close to regions of the boundary with high curvature, usually at a distance from the boundary that is one mesh size. Artificial boundary layers are thus added to the decomposition (see [5, Fig. 12 and 14]).

8. Application of our FEM scheme to the torus

The Euler-Poincaré characteristic of the torus is $\chi = 0$. Theoretically, we should obtain a cross field without critical points. But our FEM scheme gives cross field with twelve critical points, located where the Gaussian curvature is maximal (exterior) or minimal (interior), Fig. 15. Fig. 15a shows that the six critical points located on the maximal Gaussian curvature line are facing the six corresponding critical points located on the minimal Gaussian curvature line. Moreover, as the former have an index $+1/4$, and the latter an index $-1/4$, Fig. 15b, the index sum of the surface is zero, as predicted by the Poincaré-Hopf theorem.

Our FEM scheme does not reach however the asymptotic behavior ($\epsilon \to 0$) of the Ginzburg-Landau functional. It means that our penalty factor ϵ is not low enough. Otherwise, the computed cross field should not have any critical points owing to (17). Actually, the computed cross field has a lower energy (72.10) than the cross field with no critical point that could be drawn by aligning crosses with the main curvatures of the surface (84.58). The tentative polyquad decomposition shown in Fig. 15c indicates that the field computed with the Ginzburg-Landau approach tends to be more uniform, in order to reduce the Dirichlet energy. It confirms that the Dirichlet term is stronger than the penalty term.

9. Conclusion

This article has demonstrated the consistency of the Ginzburg-Landau theory to compute directional fields on arbitrary surfaces. The proposed approach relies on a physical and mathematical backgrounds. This provides proofs, analytical solutions and helps delineating fundamental mathematical properties that can be exploited in algorithms.

In particular, the Ginzburg-Landau theory states that when the coherence length ϵ is small enough, the asymptotic behavior is reached, i.e., the number of critical points of the cross field is minimal, their index is also minimal and

15

they are optimally distributed. A simple FEM scheme has been implemented to validate numerically this assertion. Cross fields have been computed on the unit disk and solutions conform with the Ginzburg-Landau theory have been found. The location of computed critical points on the 2-sphere corresponds to the solution of Whyte's problem: for a cross field they are at the summits of an anticube whereas for an asterisk field they are at the summits of a regular dodecahedron.

By weakening the boundary conditions of the Ginzburg-Landau problem, critical points are no longer repelled in the interior of the domain and can be located on the boundary, which improves the polyquad decomposition in the case of the NACA profiles.

Finally, the process is applied to the quadrangular meshing of the coastal domain around Florida peninsula, Fig. 16. Quadrangles are merged from right-angled triangles whose vertices have been spawned along the integral lines of a cross field, Fig. 17a. One sees on Fig. 17b how the edges of the recombined quadrangular elements tend to follow the cross field, and the final mesh is of satisfying quality, Fig. 18.

The input triangular mesh can be improved by using an asterisk field. This field is used to spawn vertices which are consistent with an equilateral triangular grid, Fig. 19a. The vertices tend to have the correct valence, except in some regions where the size field changes, Fig. 19b. The final triangular mesh exhibits a smoother distribution of equilateral triangles through the domain, while the mean quality $\bar{\gamma}$ has been improved to 0.9559 (from $\bar{\gamma}$ =0.9505 for the initial mesh), Fig. 20.

Further work will focus on highly improving the numerical scheme that solves Ginzburg-Landau equations, in order to make it competitive.

Acknowledgements

References

[1] C. K. Lee, S. Lo, A new scheme for the generation of a graded quadrilateral mesh, Computers & structures 52 (1994) 847–857.

[2] J.-F. Remacle, J. Lambrechts, B. Seny, E. Marchandise, A. Johnen, C. Geuzaine, Blossom-Quad: A non-uniform quadrilateral mesh generator using a minimum-cost perfect-matching algorithm, International Journal for Numerical Methods in Engineering 89 (2012) 1102–1119.

[3] D. Bommes, H. Zimmer, L. Kobbelt, Mixed-integer quadrangulation, ACM Transactions on Graphics 28 (2009) 1.

[4] F. Kälberer, M. Nieser, K. Polthier, Quadcover-surface parameterization using branched coverings, in: Computer graphics forum, volume 26, Wiley Online Library, 2007, pp. 375–384.

[5] N. Kowalski, F. Ledoux, P. Frey, A pde based approach to multidomain partitioning and quadrilateral meshing, Proceedings of the 21st international meshing roundtable (2013) 137–154.

[6] Y.-K. Lai, M. Jin, X. Xie, Y. He, J. Palacios, E. Zhang, S.-M. Hu, X. Gu, Metric-driven rosy field design and remeshing, IEEE Transactions on Visualization and Computer Graphics 16 (2010) 95–108.

[7] J. Palacios, E. Zhang, Rotational symmetry field design on surfaces, ACM Transactions on Graphics (TOG) 26 (2007) 55.

[8] N. Ray, B. Vallet, W. C. Li, B. Lévy, N-symmetry direction field design, ACM Transactions on Graphics 27 (2008) 1–13.

[9] Y. T. P. A. D. Cohen, S. M. Desbrun, Designing quadrangulations with discrete harmonic forms, in: Eurographics symposium on geometry processing, 2006, pp. 1–10.

[10] A. Vaxman, M. Campen, O. Diamanti, D. Panozzo, D. Bommes, K. Hildebrandt, M. Ben-Chen, Directional field synthesis, design, and processing, in: Computer Graphics Forum, volume 35, Wiley Online Library, 2016, pp. 545–572.

[11] D. Eppstein, Nineteen proofs of Euler's formula: $V - E + F = 2$, Information and Computer Sciences, University of California, Irvine (2009).

[12] F. Bethuel, H. Brezis, F. Hélein, Ginzburg-Landau Vortices, volume 13, Springer, 1994.

[13] M. Crouzeix, P.-A. Raviart, Conforming and nonconforming finite element methods for solving the stationary stokes equations i, Revue française d'automatique, informatique, recherche opérationnelle. Mathématique 7 (1973) 33–75.

[14] N. Ray, D. Sokolov, B. Lévy, Practical 3d frame field generation, ACM Transactions on Graphics (TOG) 35 (2016) 233.

[15] E. B. Saff, A. B. Kuijlaars, Distributing many points on a sphere, The mathematical intelligencer 19 (1997) 5–11.

[16] P. D. Dragnev, D. Legg, D. Townsend, On the separation of logarithmic points on the sphere, in: Approximation Theory X: Abstract and Classical Analysis, Vanderbilt University Press, Nashville, TN, 2002, pp. 137–144.

[17] M. Fekete, Über die verteilung der wurzeln bei gewissen algebraischen gleichungen mit ganzzahligen koeffizienten, Mathematische Zeitschrift 17 (1923) 228–249.

[18] C. Georgiadis, P.-A. Beaufort, J. Lambrechts, J.-F. Remacle, Mesh generation on the sphere using cross and asterisk fields (2017). Accepted as a research note for the IMR26.

[19] J. Jezdimirović, A. Chemin, P.-A. Beaufort, J.-F. Remacle, Elliptic Fekete points obtained by Ginzburg-Landau PDE. (2017). Accepted as a research note for the IMR26.
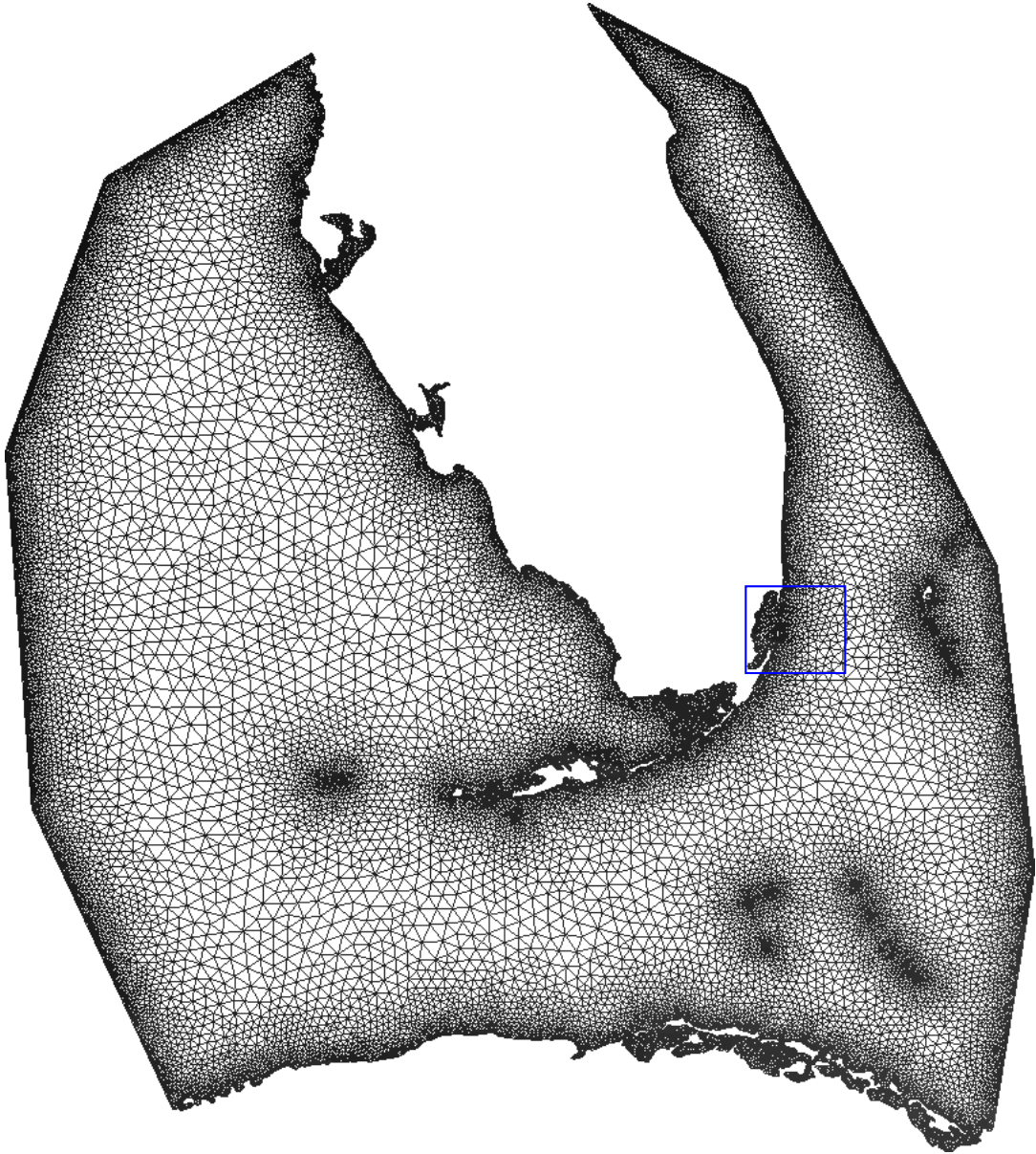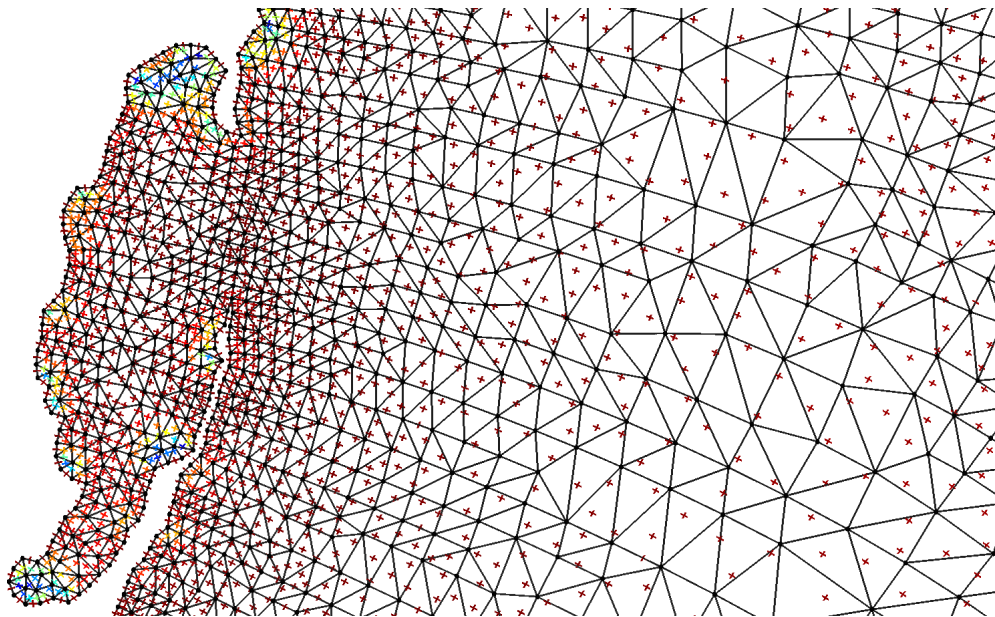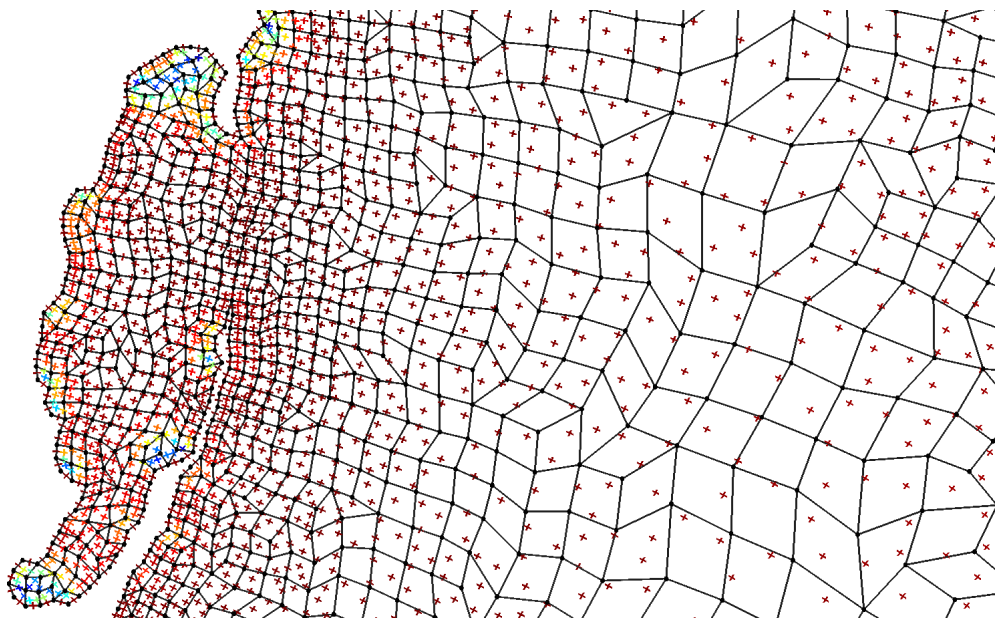
Figure 16: Florida keys: input triangular mesh ($\bar{\gamma} = 0.9504$). The blue rectangle will be enlarged.

a. Right-angled triangles from cross field.

b. Final quadrangular mesh after optimization.

Figure 17: Zoom on the Florida keys, the color map is 0 (blue) to 1 (red) and describes the norm of directions.

[20] C. Geuzaine, J.-F. Remacle, Gmsh: A 3-D finite element mesh generator with built-in pre- and post-processing facilities, International Journal for Numerical Methods in Engineering 79 (2009) 1309–1331.

Appendix A. Computing renormalized energy on a unit circle

This appendix provides an analytical form of the renormalized energy $W(X^c)$ of equation (24) for a unit disk . We first compute Φ and then prove that secont term of (23) is equal to zero in the case of a unit circle.
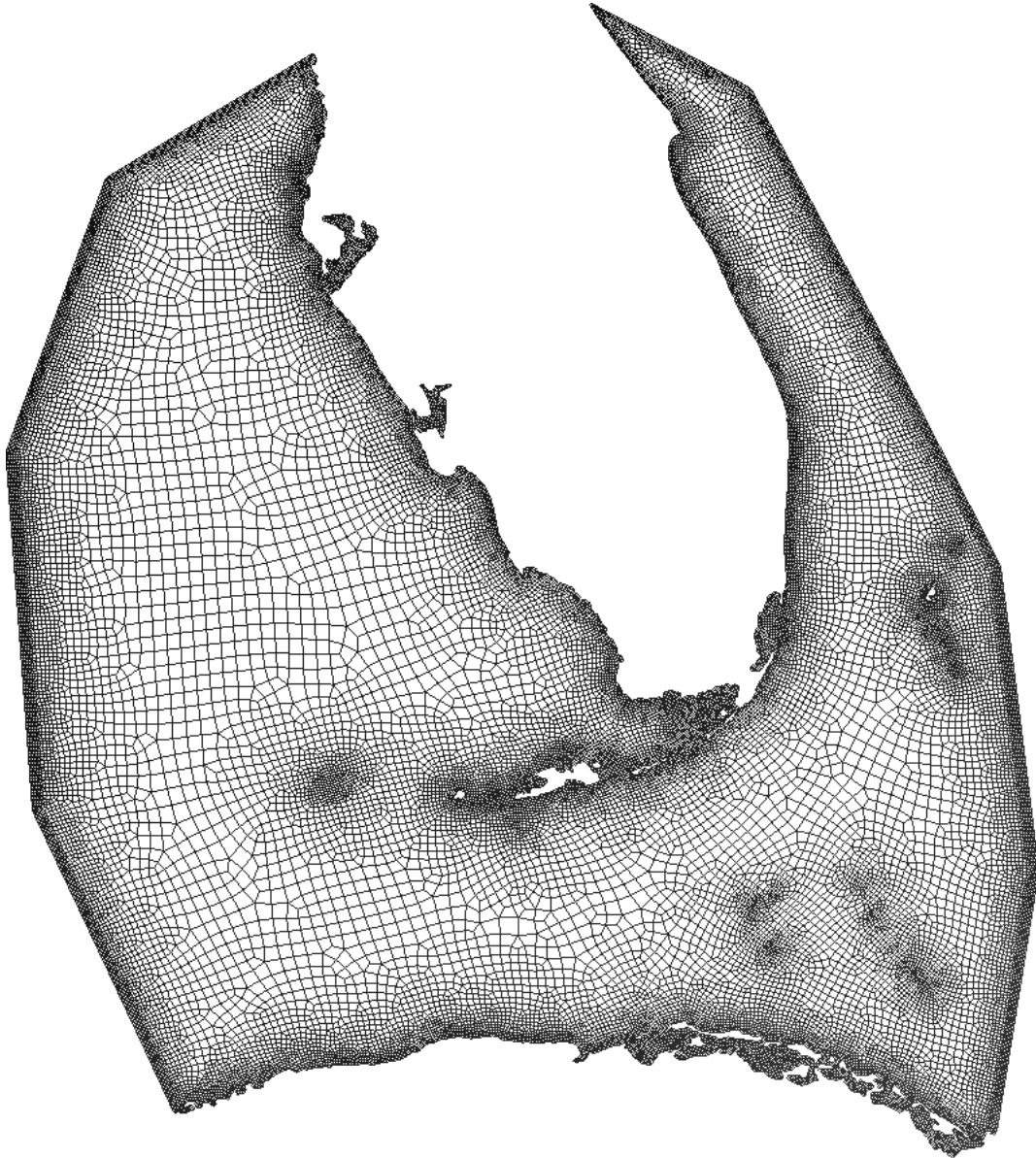
18

Figure 18: Final quadrangular mesh over the Florida keys.

Appendix A.1. Solving the Neumann problem i.e. computing $\Phi(x)$ *of Equation* (24)

Assume a unit circle S. The analytical value of f on the boundary ∂S of S is
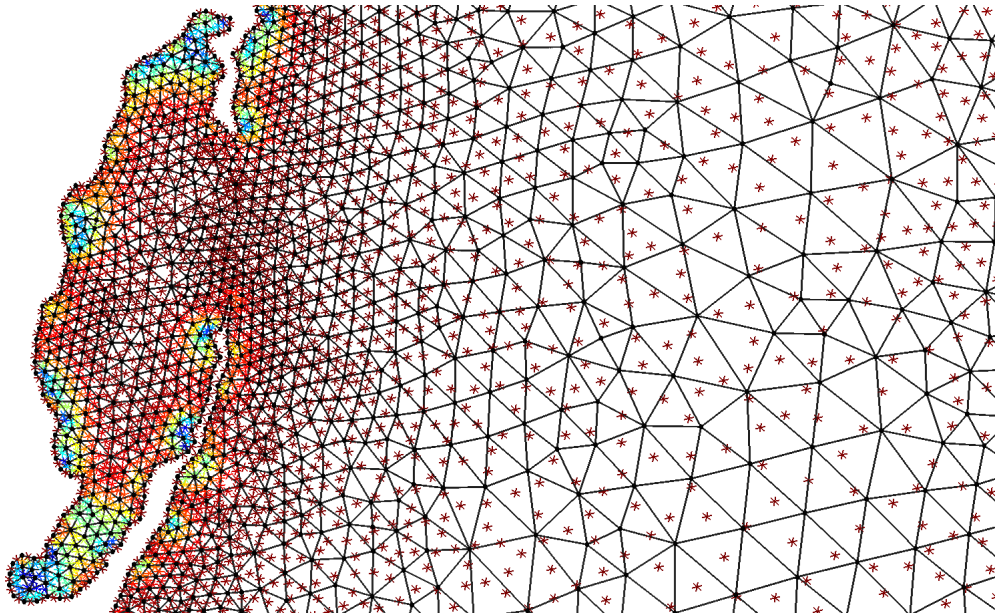
$$f = \exp(i \, d\theta) \text{ on } \partial S$$

as one direction has to be aligned with τ along the circle. The Neumann boundary condition is thus
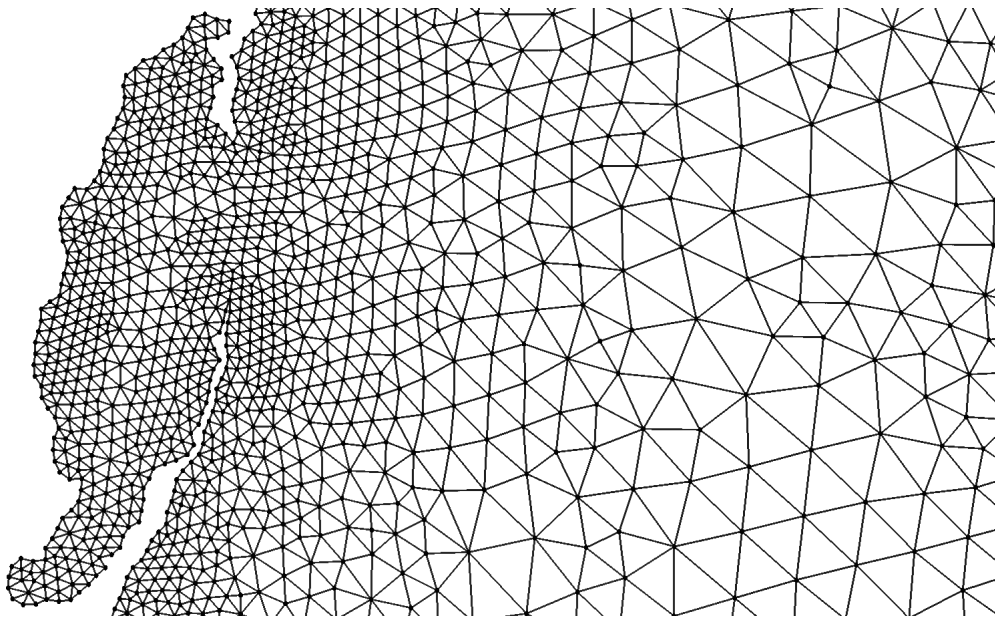
$$\frac{\partial \Phi}{\partial \nu} = d \text{ on } \partial S \tag{A.1}$$

since $f \times \nabla f \cdot \tau = d$ on ∂S. Indeed, from

$$a\bar{b} = a \cdot b - i \, a \times b, \forall a, b \in \mathbb{C}$$

19

a. Asterisk field over the new triangles.

b. New triangular mesh.

Figure 19: Zoom on the Florida keys, the color map is 0 (blue) to 1 (red) and describes the norm of directions.

and

$$\nabla f \cdot \tau = d \, i \, f \nabla \theta \cdot \tau = i \, df$$

the condition (A.1) corresponds to the imaginary part of the corresponding complex product.

a. Quality value γ of initial triangles.
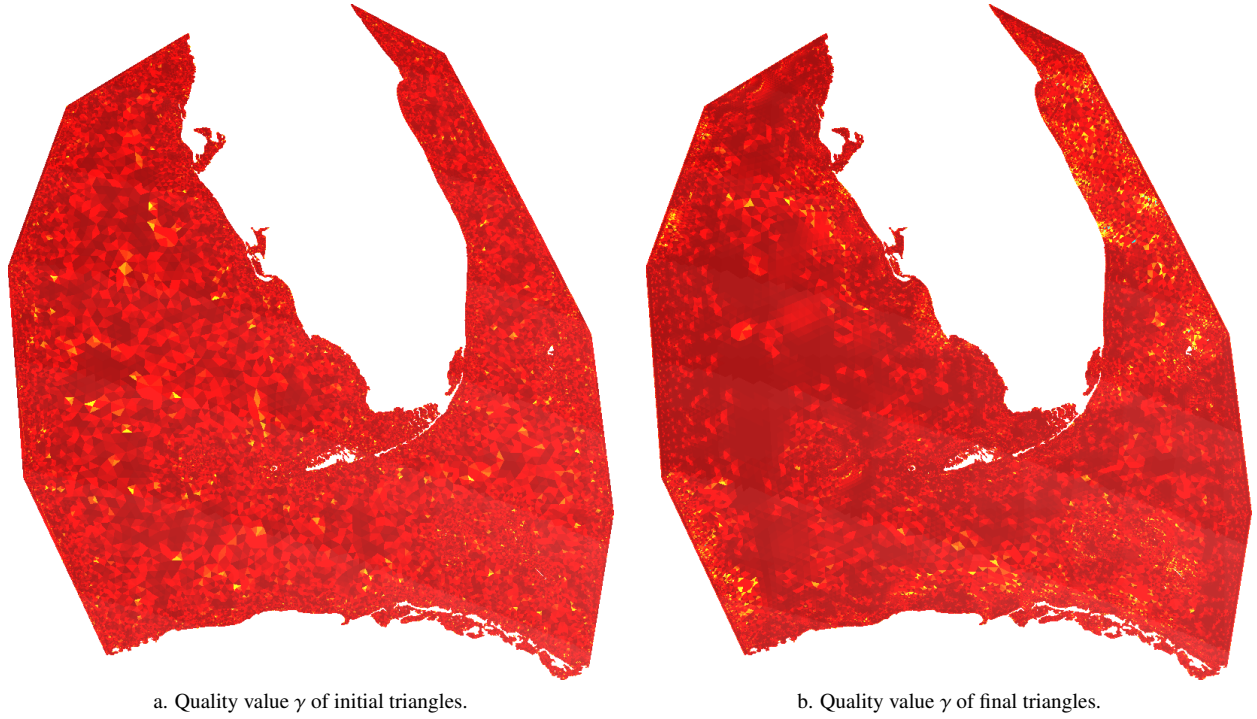
b. Quality value γ of final triangles.

Figure 20: Zoom on the Florida keys, the color map is 0 (blue) to 1 (red) and describes the quality of triangles.

The Green function of the two-dimensional Laplacian operator is part of Φ

$$\Phi^0(\mathbf{x}) = \sum_{i=1}^{d} \log |\mathbf{x} - \mathbf{x}_i^c| \tag{A.2}$$

Even if $\nabla^2 \Phi^0 = 2\pi \sum_{i=1}^{d} \delta(\mathbf{x} - \mathbf{x}_i^c)$, the flux (per unit of length) $\nabla \Phi^0 \cdot \nu$ does not correspond to (A.1). The solution Φ contains another term Φ^1. It may also be written as a sum of the contributions coming from the d critical points. Therefore,

$$\Phi = \Phi^0 + \Phi^1 = \sum_{i=1}^{d} \left(\Phi_i^0 + \Phi_i^1 \right)$$

such that

$$\begin{array}{rcl} \Phi_i^0(\mathbf{x}) & = & \log |\mathbf{x} - \mathbf{x}_i^c| \\ \nabla^2 \Phi_i^1 & = & 0 \text{ in } \mathcal{S} \\ (\nabla \Phi_i^0 + \nabla \Phi_i^1) \cdot \nu & = & 1 \text{ on } \partial \mathcal{S} \end{array} \tag{A.3}$$

Function Φ_i^1 can be written as series of circular harmonics

$$\Phi_i^1(r; \theta) = A_{i,0} + \sum_{n=1}^{\infty} r^n \left[A_{i,n} \cos(n\,\theta) + B_{i,n} \sin(n\,\theta) \right]$$

where $(r; \theta)$ are polar coordinates. We search for the solution of a Neumann problem which is defined to a constant. Setting set $A_{i,0} = 0$ assigns to zero the average of Φ_i^1. The idea is simple. We use Φ^1 which is harmonic to remove all oscillatory parts of $\nabla \Phi \cdot \nu$ along the boundary $\partial \mathcal{S}$.

Let us assume the i-th critical point is located on the x axis (the real axis), i.e. $\mathbf{x}_i^c = (r^c; 0)$ with cartesian coordinates (see Figure A.21). One has
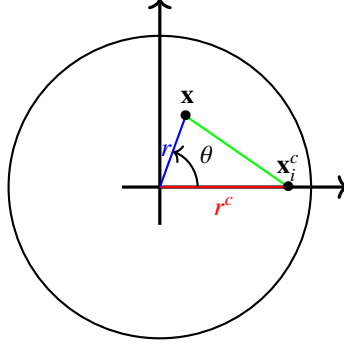
21

Figure A.21: Unit disk where the i-th critical point is depicted.

$$|\mathbf{x} - \mathbf{x}_i^c|^2 = r^2 + r^{c2} - 2rr^c \cos(\theta)$$

and

$$\left.\frac{\partial \Phi_i^0}{\partial r}\right|_{r=1} = \frac{1}{|\mathbf{x} - \mathbf{x}_i^c|} \left.\frac{\partial |\mathbf{x} - \mathbf{x}_i^c|}{\partial r}\right|_{r=1} = \frac{1 - r^c \cos \theta}{1 + r^{c2} - 2r^c \cos \theta}.$$

The last expression can be reformulated as

$$\frac{(1 + r^{c2} - 2r^c \cos \theta) + 1 - r^{c2}}{2(1 + r^{c2} - 2r^c \cos \theta)} = \frac{1 - s \cos \theta + \frac{1 - r^{c2}}{1 + r^{c2}}}{2(1 - s \cos \theta)}$$

with $s = 2r^c/(1 + r^{c2})$. Taking into account the identity

$$\frac{1}{1 - x} = \sum_{n=0}^{\infty} x^n, \quad |x| < 1,$$

we have

$$\left.\frac{\partial \Phi_i^0}{\partial r}\right|_{r=1} = \frac{1}{1 + r^{c2}} \left(1 + \left[\sum_{n=1}^{\infty} s^n (\cos \theta)^n\right] \frac{1 - r^{c2}}{2}\right) \tag{A.4}$$

and

$$\left.\frac{\partial \Phi_i^1}{\partial r}\right|_{r=1} = \sum_{n=1}^{\infty} n(A_{i,n} \cos(n\theta) + B_{i,n} \sin(n\theta)). \tag{A.5}$$

Powers of $\cos(\theta)$ appear in (A.4). In order to replace such powers by $\cos(n\,\theta)$'s like in Equation (A.5), we use a well known property of Chebyshev polynomials: $P_n(\cos(\theta)) = \cos(n\,\theta)$. We thus have

$$\cos(m\theta) = \sum_{m=0}^{n} \mathcal{P}_{mn} (\cos \theta)^n \tag{A.6}$$

where the $\mathcal{P}_{mn}$'s are the entries of the Chebyshev coefficient matrix $\mathcal{P}$. Equation (A.6) can thus be regarded as a system of equations

$$X_i = \mathcal{P}_{in} Y_n \quad , \quad X_i = \cos(i\theta) \quad , \quad Y_n = (\cos \theta)^n.$$

The system matrix $\mathcal{P}$ is lower triangular, so the system can be inverted easily

$$Y_n = \mathcal{P}_{ni}^{-1} X_i,$$

or equivalently, back with the initial notation,

$$(\cos(\theta))^n = \sum_{i=0}^{n} \mathcal{P}_{ni}^{-1} (\cos(i\theta)).$$

22

Thus,

$$\sum_{n=1}^{\infty} s^n (\cos\theta)^n = \sum_{n=1}^{\infty} s^n \sum_{i=0}^{n} \mathcal{P}_{ni}^{-1}(\cos i\theta) = \sum_{n=0}^{\infty} w_n \cos n\theta$$

with

$$w_n = \sum_{i=n}^{\infty} s^i \mathcal{P}_{in}^{-1}.$$

Finally, we get the following series for the normal derivative of Φ_i^0:

$$\left.\frac{\partial \Phi_i^1}{\partial r}\right|_{r=1} = \underbrace{\frac{1}{1+r^{c2}}\left(1 + w_0 \frac{1-r^{c2}}{2}\right)}_{W_0=1} + \sum_{n=1}^{\infty} \underbrace{\frac{1-r^{c2}}{2(1+r^{c2})}w_n}_{W_n}(\cos n\theta)$$

We get the final condition

$$\left.\frac{\partial(\Phi_i^0 + \Phi_i^1)}{\partial r}\right|_{r=1} = W_0 + \sum_{n=1}^{\infty} \left[(W_n + nA_{i,n})\cos(n\theta) + nB_{i,n}\sin(n\theta)\right]. \tag{A.7}$$

The boundary condition should be non oscillatory: So,

$$B_{i,n} = 0 \quad \text{and} \quad A_{i,n} = -\frac{W_n}{n}.$$

Finally

$$\Phi(\mathbf{x}) = \sum_{i=1}^{d}\left[\log|\mathbf{x} - \mathbf{x}_i^c| + \sum_{n=1}^{\infty} r^n A_{i,n}\cos(n\theta)\right].$$

Appendix A.2. $\int_{\partial S} \Phi\, f \times f_\tau\, ds$ is zero along a circle

We want to show that

$$\int_{\partial S} \Phi\, f \times \nabla f \cdot \tau\, ds = 0$$

when ∂S is a unit circle.

In the previous section, we have shown that

$$f \times \nabla f \cdot \tau = d$$

Besides, Φ^1 has been derived such that it is non oscillatory along the unit circle. Hence, it remains to show

$$\sum_{k=1}^{d} \int_{\partial S} \log|\mathbf{x} - \mathbf{x}_k^c|\, ds = 0$$

We can express that integral with complex variables

$$\Re\left\{\sum_{k=1}^{d} \oint_{|z|=1} \log(z - z_k^c)\, dz\right\} = 0$$

with the complex logarithm, which raises two features:

- the complex logarithm is a multivalued function

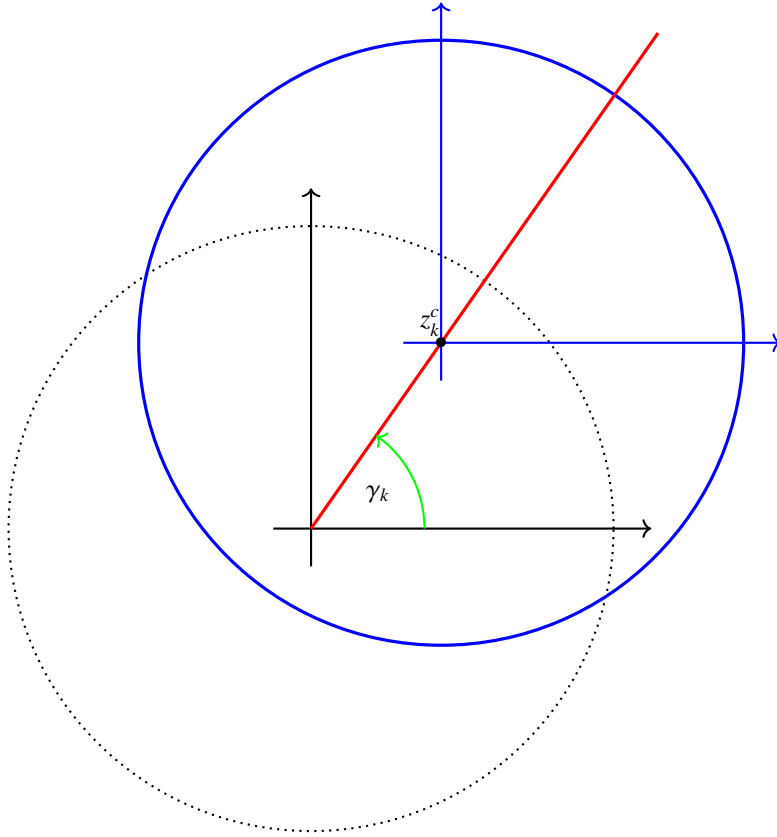- the complex logarithm has a peculiar singularity in zero

23

Figure A.22: Illustration of the k-th critical point defining a branch cut (in red) for the corresponding complex logarithm.

Those features are due to the fact that zero is a branch point. In our case, the branch points are the critical points z_k^c. A branch cut has to be drawn for each critical point. If $z_k^c = r^c \exp(i\,\gamma_k)$, the branch cut is such that $\theta \in [\gamma_k; \gamma_k + 2\pi), z = r \exp(i\,\theta) \in \mathbb{C}$ (red line on Fig. A.22).

The complex integral defines a contour integral. Complex analysis states that a contour integral is unchanged as long the curve wraps the same singularities. Hence, we change the contour ∂S (dotted circle on Fig. A.22) into another unit circle C centered in z_k^c (blue circle on Fig. A.22). We thus change the variable

$$w := z - z_k^c$$

And compute the residue of

$$\oint_C \log(w)\, dw = 2\pi i\ \exp(i\,\gamma_k)$$

which depends on the branch cut.

The d critical points z_k^c being at the same distance r^c from the origin and evenly spaced by an angles $2\pi/d$, we get

$$\sum_{k=1}^{d} \oint_{|z|=1} \log(z - z_k^c)\, dz = 2\pi i \sum_{k=1}^{d} \exp(i[\gamma_1 + (k-1)2\pi/d])$$

which is zero since the sum of $d > 1$ complex numbers corresponding to points evenly distributed along on a circle centered at the origin is zero.